Stem Cell Reports
Report
OPEN ACCESS

Embryonic Stem Cells License a High Level of Dormant Origins to Protect the Genome against Replication Stress

Xin Quan Ge,[1] Jinah Han,[2] Ee-Chun Cheng,[1] Satoru Yamaguchi,[4,5] Naoko Shima,[4] Jean-Leon Thomas,[2] and Haifan Lin[1,3,*]

[1]Yale Stem Cell Center and Department of Cell Biology
[2]Yale Cardiovascular Research Center and Department of Internal Medicine
Yale University School of Medicine, New Haven, CT 06520, USA
[3]SIAIS and School of Life Science and Technology, ShanghaiTech University, Shanghai 201210, China
[4]Department of Genetics, Cell Biology and Development, University of Minnesota, Minneapolis, MN 55455, USA
[5]Present address: General Surgical Science/Education and Research Support Center, Gunma University Graduate School of Medicine, 3-39-22 Showa-machi, Maebashi, Gunma 371-8511, Japan
*Correspondence: haifan.lin@yale.edu
http://dx.doi.org/10.1016/j.stemcr.2015.06.002

SUMMARY

Maintaining genomic integrity during DNA replication is essential for stem cells. DNA replication origins are licensed by the MCM2–7 complexes, with most of them remaining dormant. Dormant origins (DOs) rescue replication fork stalling in S phase and ensure genome integrity. However, it is not known whether DOs exist and play important roles in any stem cell type. Here, we show that embryonic stem cells (ESCs) contain more DOs than tissue stem/progenitor cells such as neural stem/progenitor cells (NSPCs). Partial depletion of DOs does not affect ESC self-renewal but impairs their differentiation, including toward the neural lineage. However, reduction of DOs in NSPCs impairs their self-renewal due to accumulation of DNA damage and apoptosis. Furthermore, mice with reduced DOs show abnormal neurogenesis and semi-embryonic lethality. Our results reveal that ESCs are equipped with more DOs to better protect against replicative stress than tissue-specific stem/progenitor cells.

INTRODUCTION

It is essential for stem cells, especially embryonic stem cells (ESCs), to maintain genome integrity. A key aspect of this is to ensure the fidelity of DNA replication. In eukaryotic genomes, DNA replication initiates at thousands of origins. Origins are licensed prior to S phase, a process that involves the recruitment of licensing factors MCM2, 3, 4, 5, 6, and 7 as double heterohexamers onto DNA (Evrin et al., 2009; Remus et al., 2009). During S phase, each MCM2–7 complex can initiate replication by acting as a helicase to unwind double-stranded DNA ahead of DNA polymerases (Bochman and Schwacha, 2009). MCM2–7 complexes are loaded onto the genome in 5- to 20-fold excess to the number utilized to initiate DNA replication. The excess MCM2–7 complexes usually remain dormant, but they initiate back-up replication forks to rescue replication when primary forks are slowed or stalled; therefore, they are called dormant origins (DOs) (Doksani et al., 2009; Ge and Blow, 2010; Ge et al., 2007; Ibarra et al., 2008). Replication forks frequently stall, for example, when encountering tightly bound protein-DNA complexes, transcription machinery, repetitive sequences, or DNA lesions (Makovets et al., 2004; Mirkin and Mirkin, 2007). Prolonged fork stalling increases the probability of fork collapse and double strand breaks, which could lead to chromosomal re-arrangements and genomic instability (Lambert et al., 2005). As a safeguard mechanism, DOs provide the first line of defense against fork stalling (Blow and Ge, 2009). Chromosomal fragile sites, which are prone to breakage upon replication stress, are shown to have lower capacity to activate DOs (Letessier et al., 2011). Mice with reduced DOs show genomic instability, age-related dysfunction, and develop tumors (Kunnev et al., 2010; Pruitt et al., 2007; Shima et al., 2007). Importantly, congenital hypomorphic MCM4 defects have been found in humans, associated with various abnormalities and elevated genomic instability (Gineau et al., 2012; Hughes et al., 2012).

Despite the importance of DOs, it is unknown whether they exist and function differently in stem cells. Here, we analyze DOs in ESCs and neural stem/progenitor cells (NSPCs) as an example of tissue stem/progenitor cells. We show that ESCs load more DOs onto the genome than NSPCs and that DOs play a significant role in defending against replication stress in both stem cell types.

RESULTS

ESCs License More DOs Than NSPCs

First, we investigated whether DOs exist in ESCs. DNA fiber assay was used to measure the density of replication forks, which involves labeling of the nascent strand DNA by BrdU pulse and visualization of labeled DNA after spreading

on microscopic slides. DNA fibers containing at least a cluster of four consecutive BrdU-incorporated forks were chosen for analysis (e.g., Figure 1A). The average fork spacing within each cluster (i.e., mean intra-cluster fork spacing) was measured. The average fork spacing of the sample was calculated from the mean intra-cluster fork spacing of over 50 clusters (Figure 1B). ESCs have an average fork spacing of ~25 kb, implying an average origin-to-origin distance of ~50 kb within replicon clusters, consistent with replicon sizes in other mammalian cells (Berezney et al., 2000; Ge et al., 2007; Kawabata et al., 2011). After treatment with hydroxyurea (HU) that inhibits ribonucleotide reductase, replication forks in ESCs slowed down by ~50% and the average fork spacing reduced to ~16 kb (Figures 1A and 1B). These results show that DOs are activated in ESCs in response to replication stress.

Next, we compared the number of DOs in ESCs and tissue stem cells, using NSPCs as an example. Because 80%–95% of the chromatin-bound MCM2–7 complexes are DOs, we quantified the complexes on the chromatin by immunoblotting (Figure 1C). ESCs contain ~2-fold more chromatin-bound MCM2–7 complexes than NSPCs. To exclude non-cycling cells from the analysis, we immunostained chromatin-bound MCM2 and analyzed the cells by flow cytometry. As licensing of replication origins starts at late mitosis and reaches the maximum at G1 phase, we quantified the chromatin-bound MCM2 in G1-phase ESCs and NSPCs. In line with the immunoblot results, ESCs contain ~2-fold more chromatin-bound MCM2–7 complexes than NSPCs (Figure 1D). Furthermore, we used super-resolution 3D structured illumination microscopy (SIM) to quantify the chromatin-bound MCM2–7 complexes. SIM reaches 120 nm resolution in the x and y axis and 300 nm in the Z axis (Figure 1E), and a double hexameric MCM2–7 complex on DNA measures 25 × 16 nm (Evrin et al., 2009; Remus et al., 2009). Hence, each focus observed by SIM contains multiple MCM2–7 complexes. Quantification of chromatin-bound MCM2, MCM3, and MCM7 foci in G1 phase cells shows approximately twice more MCM2–7 complexes in ESCs than in NSPCs (Figures 1F, upper panel, and S5A). Because the average volume of MCM foci in ESCs is larger than in NSPCs, the difference of the chromatin-bound MCM2–7 complexes between ESCs and NSPCs is likely even greater (Figure 1F, lower panel). All the above data together demonstrate that ESCs possess ~2-fold more chromatin-bound MCM2–7 complexes and therefore more DOs than NSPCs.

Finally, DNA fiber assay shows similar overall fork spacing in both ESCs and NSPCs (~26 kb; Figure 1G, left panel), suggesting a similar usage of primary origins. However, after HU treatment, average fork spacing reduces to ~16 kb in ESCs and only to ~19 kb in NSPCs (Figure 1G, right panel), confirming fewer DOs in NSPCs than ESCs.

Reducing DOs Impairs ESC Differentiation, but Not Self-Renewal

We next examined the function of DOs in ESCs by knocking down MCM5 using siRNAs. In order to reduce DOs while keeping primary origins intact, we titrated out the *Mcm5* siRNAs to achieve ~60% MCM5 knockdown in ESCs while maintaining a normal rate of cellular proliferation and DNA replication (Figures 2A, 2B, and S1A, upper panel). DNA fiber assay shows a similar average fork spacing between the siRNA-treated cells and the control, confirming that the usage of primary origins is unaffected. However, upon adding HU, activation of DOs is greatly reduced in the siRNA-treated cells (Figure S2A), and ESCs show hypersensitivity to replication inhibitors HU and aphidicolin, including a hyper-activation of DNA damage response proteins, a further reduction of the overall rate of DNA replication, and a significant increase of apoptosis (Figures 2B, 2C, and S1A, lower panel). These results demonstrate that DOs are required for ESCs to rescue replication fork stalling and to survive replication stress.

To avoid the transient effect of siRNAs, we derived ESCs from the $Mcm4^{Chaos3}$ mice that contain a point mutation within the *Mcm4* gene, resulting in the unstable MCM2–7 complexes and thus reduced DOs on chromatin (Kawabata et al., 2011). We assayed four $Mcm4^{Chaos3/Chaos3}$ ($Mcm4^{C/C}$) ESC lines and four wild-type controls ($Mcm4^{+/+}$). Immunoblotting shows a partial reduction of the chromatin-bound MCM2–7 complexes in the $Mcm4^{C/C}$ ESCs (Figure S1C). Consistent with the *Mcm5*-siRNA-treated ESCs, the overall rates of proliferation and DNA replication of the $Mcm4^{C/C}$ ESCs are normal compared with the wild-type ESCs (Figures 2D, S1D, and S1E). The $Mcm4^{C/C}$ ESCs also maintain pluripotency: there are 80%–95% of Oct4, Sox2, and SSEA-1-positive cells in the $Mcm4^{C/C}$ ESC culture, similar to the control (Figures 2E, S1F, and S1G). Expectedly, the $Mcm4^{C/C}$ ESCs are hypersensitive to replication fork inhibitors HU and aphidicolin (Figures 2F, S1H, and S1I).

Because $Mcm4^{C/C}$ ESCs maintain normal self-renewal, we examined their differentiation. As they differentiate into NSPCs, they show increased cell death and decreased expression of NSPC markers NESTIN and SOX1 (Figures 2G–2I, S2A, and S2B). In addition, they show defective differentiation toward embryoid bodies, displaying abnormal morphology and compromised expression of neuroectoderm, endoderm, and mesoderm markers (Figures 2J, 2K, and S2C). To further assess their differentiation capability in vivo, we injected them into immune-compromised mice and allowed them to form teratomas. Although the cellular composition of the $Mcm4^{C/C}$ and the wild-type ESC-derived teratomas is similar (Figure S2D), the $Mcm4^{C/C}$ ESCs generate 50% fewer teratomas and these teratomas weigh 50% less than those derived from the wild-type

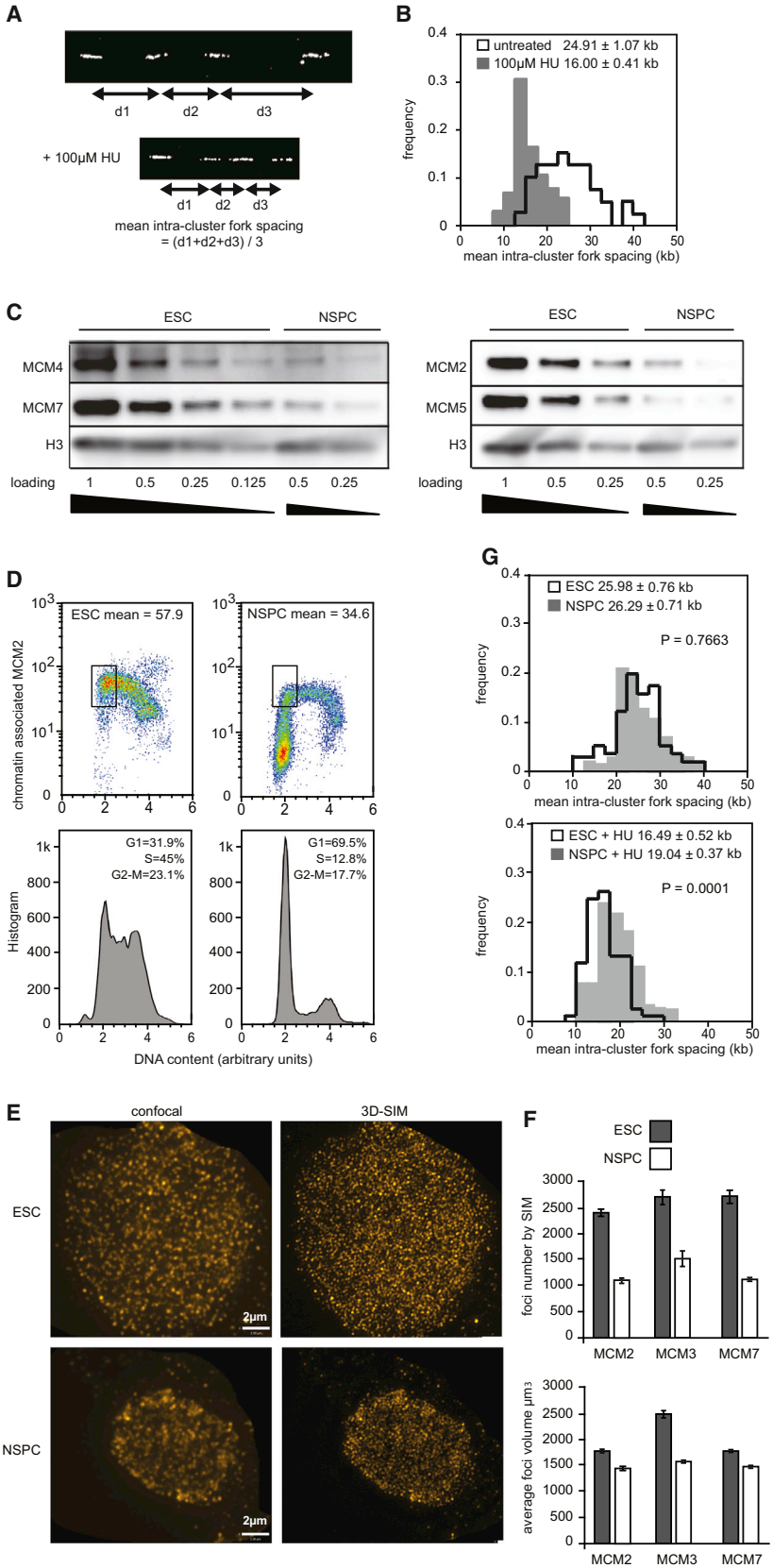

Figure 1. ESCs Possess More DOs Than NSPCs

(A and B) DNA fiber assay on mouse ESCs (CCE strain). For exclusion of artifacts arising from fork-to-fork fusion, cells were pulsed with BrdU for 10 min in the absence of HU and 20 min in the presence of HU to achieve similar replication fork length. (A) Examples of a DNA fiber containing a replicon cluster of four BrdU-labeled forks are shown. (B) Distribution of the mean intra-cluster fork spacing from >50 replicon clusters is shown. Overall fork spacing ± SEM is indicated in the chart.

(C–G) Comparisons between CCE cells derived from the 129/Sv mice and NSPCs from the E13.5 129/Sv embryo brains. (C) Immunoblotting of chromatin-bound MCM proteins with H3 as a loading control for quantification is shown. (D) Quantification of chromatin-bound MCM2 in G1-phase cells and cell-cycle distribution by FACS are shown. (E) 2D projection confocal and SIM images of chromatin-bound MCM2, MCM3, and MCM7 in G1 phase cells are shown. (F) Quantification of chromatin-bound MCM foci number and average focus volume imaged by SIM are shown. Error bars represent SEM of three independent experiments. (G) DNA fiber analysis of NSPCs and ESCs is shown. Cells were incubated with 100 μM HU for 4 hr before BrdU pulse. Overall fork spacing ± SEM from >50 replicon clusters is indicated. p values are from two-tailed t test.

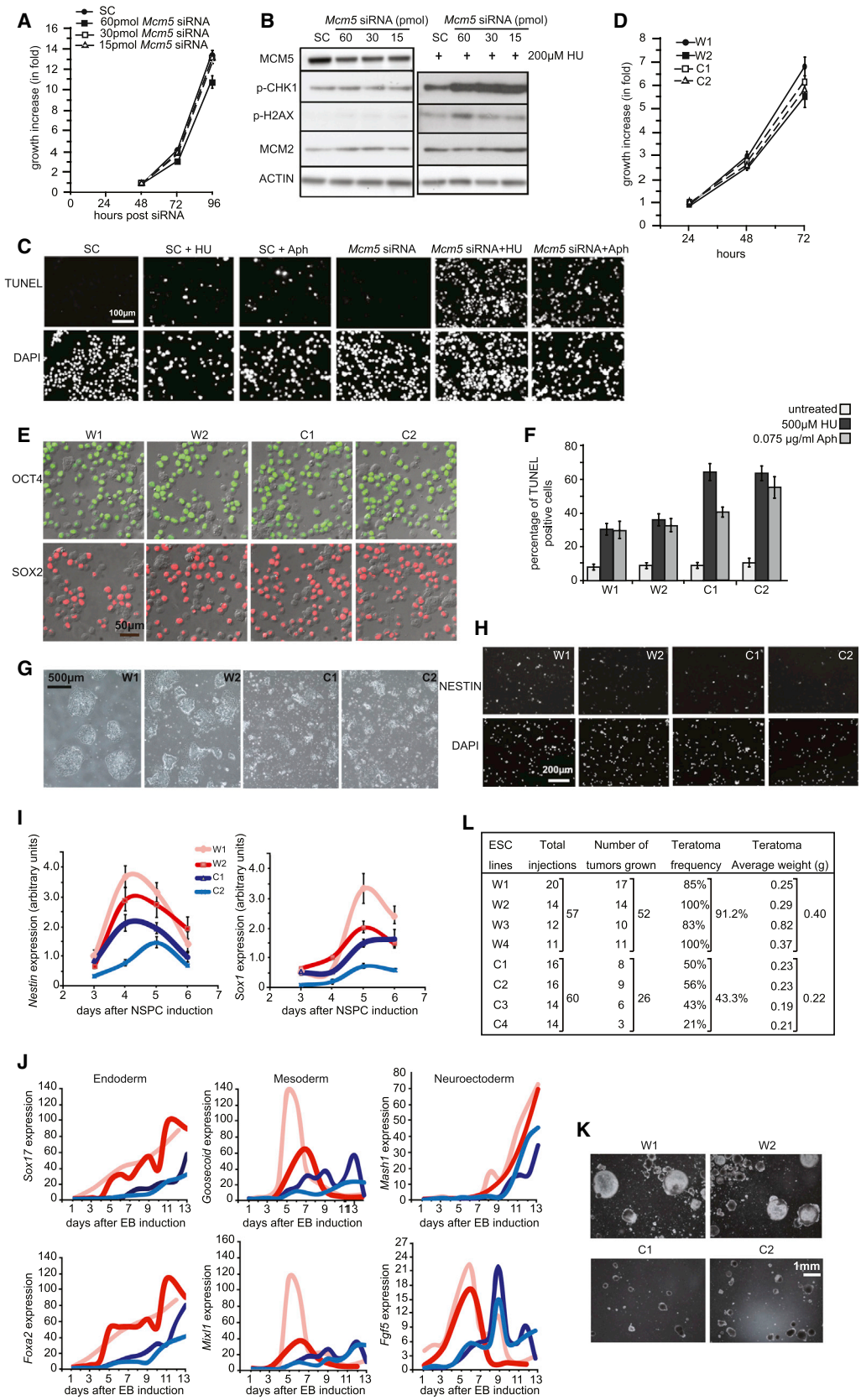

ESC lines	Total injections		Number of tumors grown		Teratoma frequency		Teratoma Average weight (g)	
W1	20	57	17	52	85%	91.2%	0.25	0.40
W2	14		14		100%		0.29	
W3	12		10		83%		0.82	
W4	11		11		100%		0.37	
C1	16	60	8	26	50%	43.3%	0.23	0.22
C2	16		9		56%		0.23	
C3	14		6		43%		0.19	
C4	14		3		21%		0.21	

(legend on next page)

controls (Figures 2L and S2E). Together, these data suggest that, upon reduction of DOs, ESCs maintain normal self-renewal but are impaired in differentiation. This is consistent with our observation that ESCs load more DOs than NSPCs. As a result, the self-renewal of ESCs is more robust against DO reduction than differentiation.

Reducing DOs Impairs ESC Differentiation to NSPCs

We further investigated the differentiation of the *Mcm4*$^{C/C}$ ESCs into NSPCs. *Mcm4*$^{C/C}$ ESC-derived NSPCs show hyper-activation of phosphorylated CHK1, P53, and H2AX and increased apoptosis (CASPASE 3 cleavage and 3-fold increase in TUNEL staining; Figures 3A, 3B, and S3A–S3C). Addition of caffeine, an ATM/ATR inhibitor, or the CASPASE inhibitor Z-VAD-FMK during NSPC differentiation largely rescued the differentiation efficiency, as shown by the increased expression of NESTIN and SOX1 (Figures 3C and S3C). The partial nature of the rescue could be due to the key role of ATR kinase during DNA replication and cell-cycle progression (Jirmanova et al., 2005; Ruzankina et al., 2007). Despite this, the above data clearly illustrate a functional relationship between reduced DOs and impaired neural differentiation of the *Mcm4*$^{C/C}$ ESCs due to elevated DNA damage response and cell death. The defect in the neural differentiation of the *Mcm4*$^{C/C}$ ESCs is likely due to compromised survival of differentiating cells.

To confirm our in vitro findings on neural differentiation, we isolated NSPCs from the *Mcm4*$^{C/C}$ mice during embryogenesis. NSPCs from the forebrain of the E13.5 *Mcm4*$^{C/C}$ embryos generated 50% fewer neurospheres than the wild-type NSPCs, even though both expressed similar level of NESTIN and SOX2 (Figures 3D, S3D, and S3E). In addition, NSPCs from the *Mcm4*$^{C/C}$ embryos lost clonogenic ability after four to six passages, whereas the wild-type NSPCs continue to form neurospheres (Figure 3E). DNA fiber assay revealed a significant lack of DOs in the *Mcm4*$^{C/C}$ NSPCs as compared with wild-type NSPCs (Figure 3F). Furthermore, there is increased cell death in the *Mcm4*$^{C/C}$ neurosphere culture and a blockage of these NSPCs at the G2-M phase (Figures 3G and S3F). Elevated DNA damage markers γH2AX, 53BP1, and phospho-P53 were also observed in the *Mcm4*$^{C/C}$ NSPCs (Figures 3H and 3I). Together, these data show abnormal proliferation and differentiation of the NSPCs in the *Mcm4*$^{C/C}$ embryonic mice brains.

Reduction of DOs Impairs Embryonic Neurogenesis and Compromises Embryonic Viability

To investigate the in vivo properties of *Mcm4*$^{C/C}$ NSPCs, we examined different stages of neurogenesis in the *Mcm4*$^{C/C}$ embryos. At E13.5 and E15.5, *Mcm4*$^{C/C}$ embryos show a reduction in the size of the ventral forebrain and the cortex compared to the wild-type (Figures 4A–4C). The discrete atrophy of ganglionic eminences and the thinning of cortex indicate that early neurogenesis is globally impaired in the *Mcm4*$^{C/C}$ embryos. The ventricular layer of the PAX6^{+} radial glia cells, i.e., neural stem cells, is however of similar size in the *Mcm4*$^{C/C}$ and wild-type embryos (Figure 4D, upper panel), suggesting that the formation and self-renewal of neural stem cells are not significantly altered by the partial loss of MCM4 function. In contrast, the number of intermediate progenitor cells (TBR2^{+}) in the cortical wall of the E13.5 *Mcm4*$^{C/C}$ embryos is significantly reduced compared to the wild-type (Figure 4D, middle panel), indicating a defect in neural stem cell differentiation and/or migration during early neurogenesis. Intermediate progenitor cells proliferate rapidly and migrate to give rise to post-mitotic neurons of the cerebral cortex. Consistently, the number of early-born post-mitotic neurons (TBR1^{+}) was reduced in the cortical plate of the E15.5 *Mcm4*$^{C/C}$ brains (Figure 4D, lower panel). Furthermore, the *Mcm4*$^{C/C}$ mutants displayed anomalies in cell proliferation and survival within the cortex (Figure 4E): a reduction of mitotic cells

Figure 2. Reducing DOs Impairs ESC Differentiation

(A) CCE cell proliferation at 48–96 hr after transfection with a serial dilution of *Mcm5* siRNA. SC, scrambled siRNA. ~90% transfection efficiency is achieved.

(B) Immunoblotting of total cell lysate at 72 hr after *Mcm5* siRNA transfection. Fifteen picomoles *Mcm5* siRNA knocked down MCM5 and had no effect on cell growth or DNA replication; hence, it was used for further analysis.

(C) TUNEL assay of ESCs after treatment with 500 μM HU or 0.075 μg/ml aphidicolin (Aph) for 48 hr. Fifteen picomoles *Mcm5* or scrambled siRNA was transfected into the cells 72 hr prior to the HU and Aph treatment.

(D–K) Assays on *Mcm4*$^{C/C}$ ESCs (C1 and C2) and wild-type *Mcm4*$^{+/+}$ ESCs (W1 and W2). (D) Cell proliferation rate analyzed over 72 hr is shown. (E) Overlay of OCT4 or SOX2 immunofluorescence images with DIC images is shown. OCT4- or SOX2-negative cells, larger than ESCs, are mostly MEF contamination in the ESC culture. (F) TUNEL assay of ESCs after treatment with HU or Aph for 48 hr is shown. (G and H) DIC images and immunofluorescence of NESTIN, respectively, of NSPCs at 96 hr after induced differentiation from ESCs are shown. (I) qRT-PCR analysis of *Nestin* and *Sox1* expression during induced NSPC differentiation from ESCs is shown. (J) qRT-PCR data of the expression of three germ layer markers from days 1 to 13 during embryoid body (EB) differentiation from ESCs are shown. (K) DIC images of EBs at day 13 after induced differentiation from ESCs are shown.

(L) Frequency and average weight of teratomas generated from the wild-type (W1–W4) and *Mcm4*$^{C/C}$ (C1–C4) ESCs.

Error bars in (A), (D), (F), (I), and (J) all represent SEM of three independent experiments. See also Figures S1 and S2.

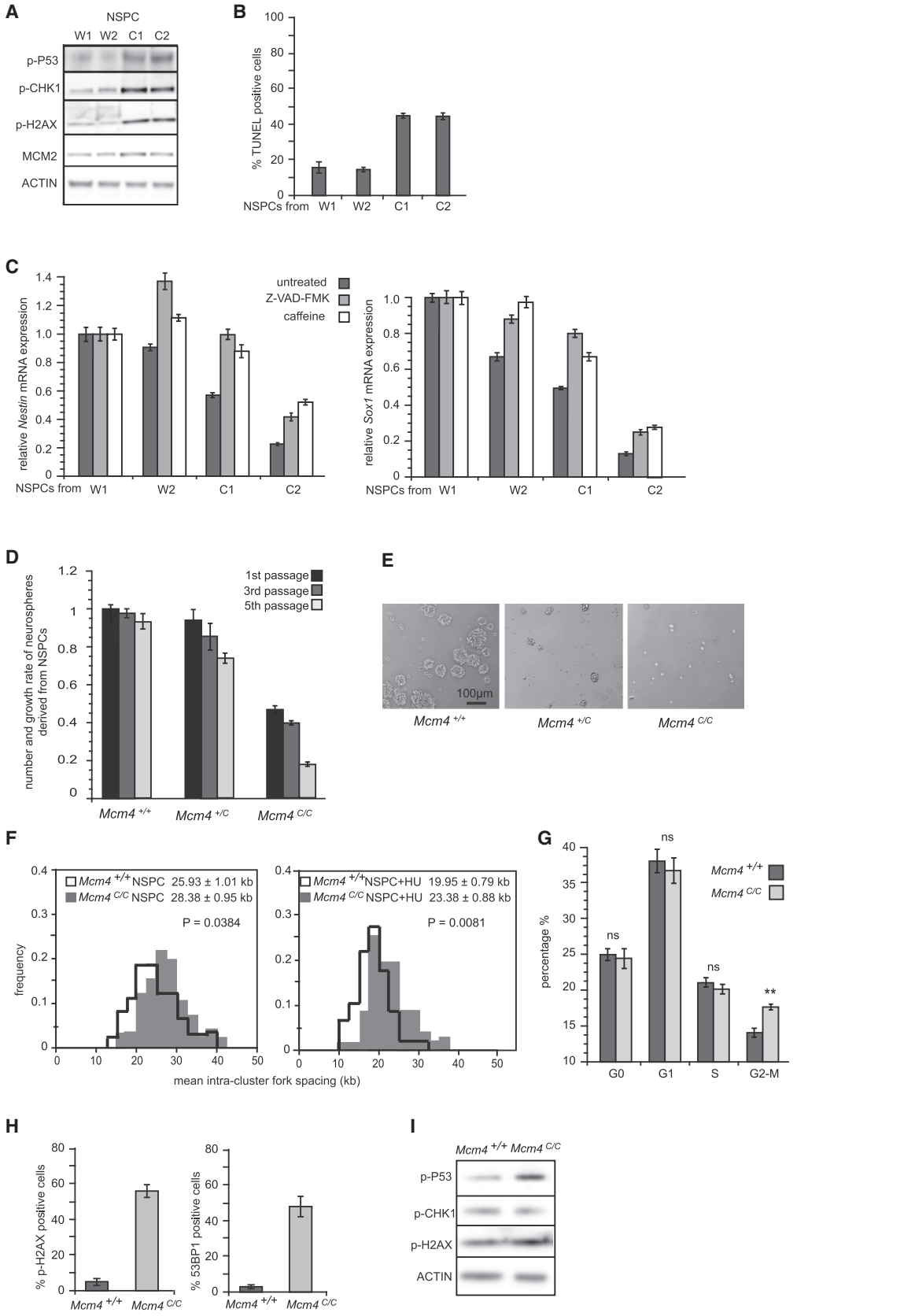

(legend on next page)

(phospho-HISTONE H3$^+$) and an increase of apoptotic cells (cleaved-CASPASE3$^+$) were detected in the sub-ventricular and intermediate zones, suggesting that cell death contributes initially to the attrition of intermediate progenitor cell pool and then to the reduction of cortical neurons. Consequently, a thinning of the cerebral cortex was observed in the E19.5 *Mcm4*$^{C/C}$ brains (Figure S4A). However, at this late stage of development, intermediate progenitor cell formation has recovered and the *Mcm4*$^{C/C}$-caused defects in neurogenesis other than cortex were no longer detectable, likely due to tissue homeostasis during development (Figure S4B).

Beyond neurogenic defects, only 40% of *Mcm4*$^{C/C}$ mice are viable (Figure S4C). Because the homozygotes are present at the correct ratio at E13.5, E15.5, and E19.9, the *Mcm4*$^{C/C}$ fetus likely dies shortly after birth. The semi-lethality of the *Mcm4*$^{C/C}$ mice is consistent with the in vitro differentiation defect of the *Mcm4*$^{C/C}$ ESCs.

DISCUSSION

We have demonstrated that ESCs recruit ~2-fold more DOs onto the genome than NSPCs. Upon reduction of DOs, the self-renewal of ESCs is unaffected, whereas their differentiation including toward NSPCs is impaired. This is due to a further reduction of DOs in NSPCs, presumably below the threshold required to rescue the endogenous fork stalling during DNA replication (Figure 4F). As a result, DNA damage is accumulated and cell death incurs, eventually leading to impaired neurogenesis in the *Mcm4*$^{C/C}$ mice. ESCs have been shown to employ unique mechanisms to maintain a more-stable genome than somatic cells, including efficient DNA repair, elimination of damaged cells, antioxidant defense, and suppression of mutagenesis (Giachino et al., 2013). Our study adds a new dimension to these unique properties by showing that ESCs use more DOs to effectively protect their genomes from replication stress and ensure their genome integrity.

It remains elusive how ESCs recruit a larger number of DOs than tissue stem/progenitor cells during DNA licensing. It is possible that ESCs express a higher level of proteins that mediate DNA licensing. Alternatively, it could be due to their open and hyper-dynamic chromatin structure (Mattout and Meshorer, 2010), which facilitates MCM2–7 loading (Miotto and Struhl, 2010; Sugimoto et al., 2011; Swarnalatha et al., 2012; Wong et al., 2010).

Because NSPCs possess fewer DOs than ESCs, when DOs are reduced, neurogenesis is more severely affected. Our findings may be related to the severe neurogenic defect in the Meier-Gorlin syndrome patients, who are characterized by mutations in replication licensing components and reduction in origin licensing (Bicknell et al., 2011; Kerzendorfer et al., 2013). In addition to NSPCs, other tissue stem/progenitor cells may possess fewer DOs than ESCs, because *Mcm4*$^{C/C}$ ESCs display broad in vitro differentiation defects. The neurogenic defect together with other organ abnormalities could collectively contribute to the semi-embryonic lethality of the *Mcm4*$^{C/C}$ mice. Future studies in other tissue stem cells in the *Mcm4*$^{C/C}$ mice will allow further understanding of the growth retardation and other deficiencies associated with the hypomorphic MCM4 conditions in human patients.

EXPERIMENTAL PROCEDURES

The *Mcm4*$^{chaos3/chaos3}$ and wild-type mouse ESC lines were derived from the blastocysts by crossing the *Mcm4*$^{chaos3/+}$ mice. They were maintained on MEF feeder in standard ESC culture medium. CCE mouse ESCs were grown without feeder. siRNA was transfected into ESCs by Lipofectamine 2000 according to manufacturer's instructions. NSPCs were isolated from the forebrain of E13.5 mice and cultured as described in Supplemental Information. Neurosphere culture on day 6 was dissociated into single cells and plate at 1,000 cells/ml to initiate clonal

Figure 3. Reducing DOs Impairs the Differentiation of NSPCs

(A–C) Analysis of the NSPC differentiation from the *Mcm4*$^{+/+}$ (W1 and W2) and *Mcm4*$^{C/C}$ (C1 and C2) ESCs. (A) Immunoblot of the NSPC total lysate is shown. (B) TUNEL assay on NSPCs at 96 hr after induced differentiation is shown. (C) qRT-PCR of *Nestin* and *Sox1* expression in NSPCs is shown. Treatment with caffeine (4 mM) or Z-VAD-FMK (40 μM) started at 48 hr after induction, and NSPCs were harvested at 96 hr for analysis.

(D–I) Analysis of neurospheres clonally derived from NSPCs isolated from the E13.5 mouse forebrain. (D) Neurospheres were passaged every 6 days to give a new round of clonogenic assay. Number and growth rate of neurospheres were measured by counting the neurospheres and the total number of cells at each passage. Error bars represent SEM from four independent experiments and each experiment containing five embryos of each genotype. (E) Representative images of neurospheres at fifth passage are shown. (F) DNA fiber analysis is shown. Cells were treated with 100 μM HU for 4 hr before analysis. Overall average fork spacing ± SEM from >50 replicon clusters is shown. p values are from two-tailed t test. (G) Cell-cycle analysis of neurospheres at fifth passage by FACS after pyronin Y and DAPI staining is shown. Note G2-M blockage of the cells in the *Mcm4*$^{C/C}$ neurospheres. Two-tailed t test: non-significant (ns); $p < 0.005$ (**). (H) Immunofluorescence quantifying the percentage of γH2AX or 53BP1 positive cells in neurospheres is shown. (I) Immunoblot of total cell lysate of neurospheres is shown.

Error bars in (B), (C), (G), and (H) all represent SEM of three independent experiments. See also Figure S3.

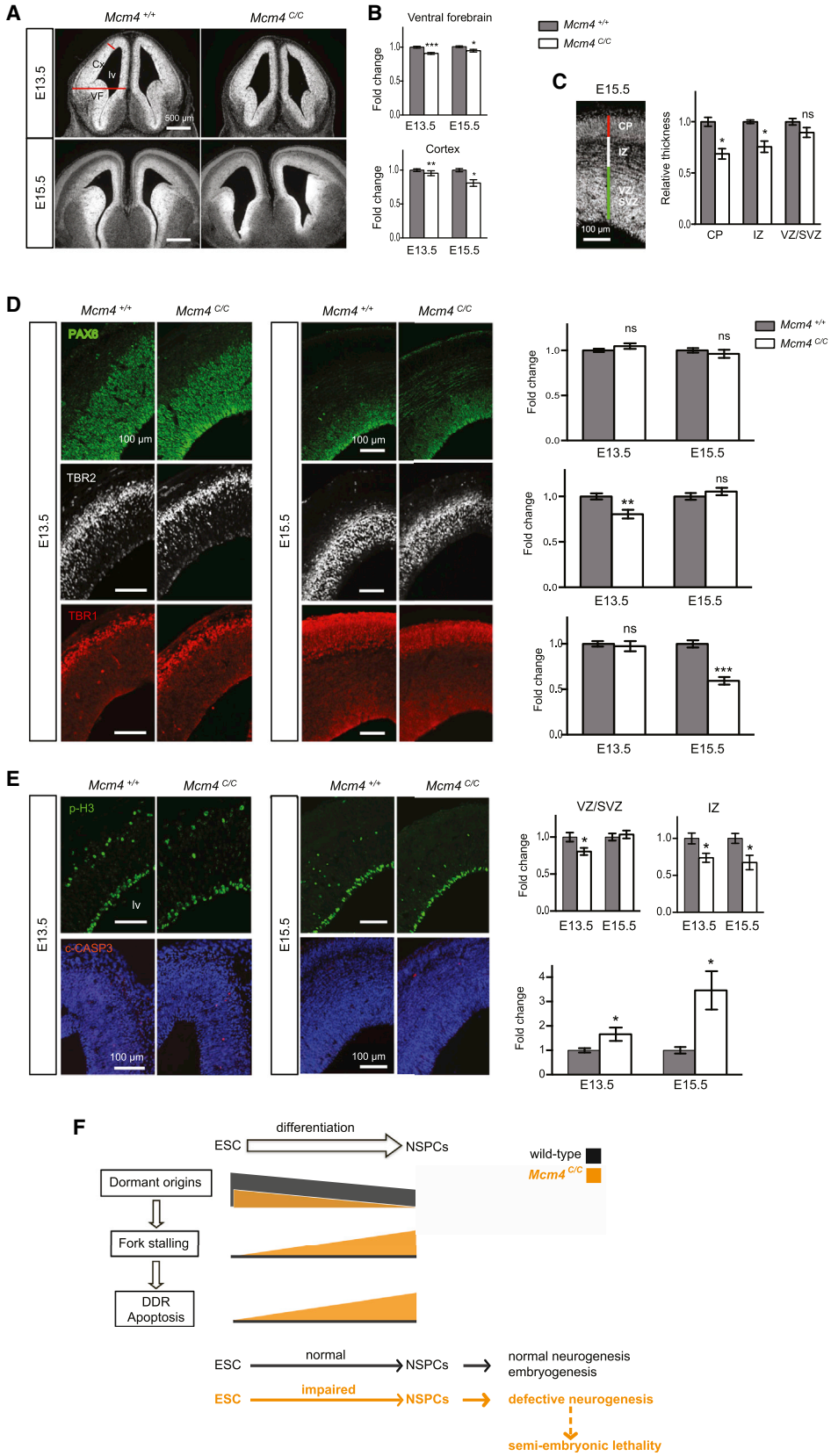

(legend on next page)

neurosphere assays. DNA fiber, chromatin-bound MCMs analysis by immunoblotting, and FACS were carried out as previously described (Ge et al., 2007). Embryonic brains from the E13.5, 15.5, and 19.5 mice were dissected, cryosectioned, and immunostained with various antibodies, including TBR2, P-H3, and cleaved-CASPASE 3 where positive cells were counted and PAX6 and TBR1 where the thickness of cell layer was measured. The rate of DNA synthesis was measured by pulse labeling cells with Click-iT EdU Alexa Fluor 647 Flow Cytometry kit (Invitrogen) according to manufacturer's instruction. Cell growth rate was assayed with the alamarBlue CellViability Reagent (Invitrogen), and apoptosis was assayed by ApopTag Fluorescein In Situ Apoptosis Detection Kit (Millipore) according to the manufacturer's instructions. NSPC differentiation was performed as previously described using the N2B27 medium (Ying et al., 2003). Embryoid body differentiation was achieved by hanging drop method (Jackson et al., 2010). The differentiation efficiency into the ectoderm, mesoderm, and endoderm was assessed by qRT-PCR using lineage-specific primers (*Nestin*, *Sox1*, *Sox17*, *Goosecoid*, *Mash1*, *Fgf5*, *Mixl1*, and *Foxa2*). For imaging of the chromatin-bound MCM foci, cells were synchronized by thymidine followed by nocodazole. Delta Vision OMX imaging system (Applied Precision) was used to collect 3D images, followed by analysis with Volocity (PerkinElmer), where a threshold-based segmentation was applied.

SUPPLEMENTAL INFORMATION

Supplemental Information includes Supplemental Experimental Procedures and four figures and can be found with this article online at http://dx.doi.org/10.1016/j.stemcr.2015.06.002.

AUTHOR CONTRIBUTIONS

X.Q.G. designed and performed the experiments and wrote the manuscript. J.H. and J.-L.T. did embryonic brain analysis. E.-C.C. conducted teratoma assay. S.Y. and N.S. provided *Mcm4*^{chaos3} and wild-type ESCs. H.L. provided guidance on the project and revised the manuscript.

ACKNOWLEDGMENTS

We thank Felix Rivera-Molina for assistance with SIM. This work was funded by a grant from the Connecticut Stem Cell Research Fund (10SCA05) to X.Q.G. and the G. Harold and Leica Y. Mathers Award to H.L.

Received: January 5, 2015
Revised: June 12, 2015
Accepted: June 13, 2015
Published: July 16, 2015

REFERENCES

Berezney, R., Dubey, D.D., and Huberman, J.A. (2000). Heterogeneity of eukaryotic replicons, replicon clusters, and replication foci. Chromosoma *108*, 471–484.

Bicknell, L.S., Bongers, E.M., Leitch, A., Brown, S., Schoots, J., Harley, M.E., Aftimos, S., Al-Aama, J.Y., Bober, M., Brown, P.A., et al. (2011). Mutations in the pre-replication complex cause Meier-Gorlin syndrome. Nat. Genet. *43*, 356–359.

Blow, J.J., and Ge, X.Q. (2009). A model for DNA replication showing how dormant origins safeguard against replication fork failure. EMBO Rep. *10*, 406–412.

Bochman, M.L., and Schwacha, A. (2009). The Mcm complex: unwinding the mechanism of a replicative helicase. Microbiol. Mol. Biol. Rev. *73*, 652–683.

Doksani, Y., Bermejo, R., Fiorani, S., Haber, J.E., and Foiani, M. (2009). Replicon dynamics, dormant origin firing, and terminal fork integrity after double-strand break formation. Cell *137*, 247–258.

Evrin, C., Clarke, P., Zech, J., Lurz, R., Sun, J., Uhle, S., Li, H., Stillman, B., and Speck, C. (2009). A double-hexameric MCM2-7 complex is loaded onto origin DNA during licensing of eukaryotic DNA replication. Proc. Natl. Acad. Sci. USA *106*, 20240–20245.

Ge, X.Q., and Blow, J.J. (2010). Chk1 inhibits replication factory activation but allows dormant origin firing in existing factories. J. Cell Biol. *191*, 1285–1297.

Figure 4. Reducing DOs Impairs Embryonic Neurogenesis and Affects Embryonic Viability

(A and B) Coronal sections of the *Mcm4*$^{+/+}$ and *Mcm4*$^{C/C}$ embryonic forebrain. (A) Phase contrast views are shown. Red lines show width of ventral forebrain (VF) and thickness of cortex (Cx). (B) Quantification of forebrain size is shown.

(C) DAPI staining and measurement of the E15.5 cortex: ventricular/sub-ventricular zone (VZ/SVZ); intermediate zone (IZ); and cortical plate (CP).

(D) Cortex coronal sections with immunolabeling of VZ/SVZ stem/progenitor cells (PAX6^{+}), intermediate progenitor cells (TBR2^{+}), and early born, deep-layer cortical neurons (TBR1^{+}).

(E) Immunolabeling of phospho-H3 and cleaved-CASPASE 3 (c-CASP3) cells on cortex coronal sections. lv, lateral ventricles. Error bars represent SEM of three independent experiments comprising in total five *Mcm4*$^{+/+}$ and four *Mcm4*$^{C/C}$ embryos at E13.5 and seven *Mcm4*$^{+/+}$ and seven *Mcm4*$^{C/C}$ embryos at E15.5. Two-tailed t test: ns; $p < 0.05$ (*); $p < 0.005$ (**); $p < 0.0005$ (***).

(F) Model. Black and orange colors indicate the conditions of the wild-type and the partial depletion of DOs (as in the *Mcm4*$^{C/C}$ mice), respectively. In the wild-type ESCs, DOs initiate back-up replication forks to rescue fork stalling and maintain genome integrity. ESCs possess a greater number of DOs than NSPCs. Upon reduction of DO, there is a further reduction of DOs in the NSPCs, likely reaching the threshold required to rescue the endogenous fork stalling during DNA replication. As a result, DNA damage is accumulated and cell death incurs, eventually impairing NSPC proliferation and differentiation. This explains the neurogenic defect in the *Mcm4*$^{C/C}$ embryos, which could contribute to the semi-embryonic lethality of the *Mcm4*$^{C/C}$ mice.

See also Figure S4.

Ge, X.Q., Jackson, D.A., and Blow, J.J. (2007). Dormant origins licensed by excess Mcm2-7 are required for human cells to survive replicative stress. Genes Dev. *21*, 3331–3341.

Giachino, C., Orlando, L., and Turinetto, V. (2013). Maintenance of genomic stability in mouse embryonic stem cells: relevance in aging and disease. Int. J. Mol. Sci. *14*, 2617–2636.

Gineau, L., Cognet, C., Kara, N., Lach, F.P., Dunne, J., Veturi, U., Picard, C., Trouillet, C., Eidenschenk, C., Aoufouchi, S., et al. (2012). Partial MCM4 deficiency in patients with growth retardation, adrenal insufficiency, and natural killer cell deficiency. J. Clin. Invest. *122*, 821–832.

Hughes, C.R., Guasti, L., Meimaridou, E., Chuang, C.H., Schimenti, J.C., King, P.J., Costigan, C., Clark, A.J., and Metherell, L.A. (2012). MCM4 mutation causes adrenal failure, short stature, and natural killer cell deficiency in humans. J. Clin. Invest. *122*, 814–820.

Ibarra, A., Schwob, E., and Méndez, J. (2008). Excess MCM proteins protect human cells from replicative stress by licensing backup origins of replication. Proc. Natl. Acad. Sci. USA *105*, 8956–8961.

Jackson, M., Taylor, A.H., Jones, E.A., and Forrester, L.M. (2010). The culture of mouse embryonic stem cells and formation of embryoid bodies. Methods Mol. Biol. *633*, 1–18.

Jirmanova, L., Bulavin, D.V., and Fornace, A.J., Jr. (2005). Inhibition of the ATR/Chk1 pathway induces a p38-dependent S-phase delay in mouse embryonic stem cells. Cell Cycle *4*, 1428–1434.

Kawabata, T., Luebben, S.W., Yamaguchi, S., Ilves, I., Matise, I., Buske, T., Botchan, M.R., and Shima, N. (2011). Stalled fork rescue via dormant replication origins in unchallenged S phase promotes proper chromosome segregation and tumor suppression. Mol. Cell *41*, 543–553.

Kerzendorfer, C., Colnaghi, R., Abramowicz, I., Carpenter, G., and O'Driscoll, M. (2013). Meier-Gorlin syndrome and Wolf-Hirschhorn syndrome: two developmental disorders highlighting the importance of efficient DNA replication for normal development and neurogenesis. DNA Repair (Amst.) *12*, 637–644.

Kunnev, D., Rusiniak, M.E., Kudla, A., Freeland, A., Cady, G.K., and Pruitt, S.C. (2010). DNA damage response and tumorigenesis in Mcm2-deficient mice. Oncogene *29*, 3630–3638.

Lambert, S., Watson, A., Sheedy, D.M., Martin, B., and Carr, A.M. (2005). Gross chromosomal rearrangements and elevated recombination at an inducible site-specific replication fork barrier. Cell *121*, 689–702.

Letessier, A., Millot, G.A., Koundrioukoff, S., Lachagès, A.M., Vogt, N., Hansen, R.S., Malfoy, B., Brison, O., and Debatisse, M. (2011). Cell-type-specific replication initiation programs set fragility of the FRA3B fragile site. Nature *470*, 120–123.

Makovets, S., Herskowitz, I., and Blackburn, E.H. (2004). Anatomy and dynamics of DNA replication fork movement in yeast telomeric regions. Mol. Cell. Biol. *24*, 4019–4031.

Mattout, A., and Meshorer, E. (2010). Chromatin plasticity and genome organization in pluripotent embryonic stem cells. Curr. Opin. Cell Biol. *22*, 334–341.

Miotto, B., and Struhl, K. (2010). HBO1 histone acetylase activity is essential for DNA replication licensing and inhibited by Geminin. Mol. Cell *37*, 57–66.

Mirkin, E.V., and Mirkin, S.M. (2007). Replication fork stalling at natural impediments. Microbiol. Mol. Biol. Rev. *71*, 13–35.

Pruitt, S.C., Bailey, K.J., and Freeland, A. (2007). Reduced Mcm2 expression results in severe stem/progenitor cell deficiency and cancer. Stem Cells *25*, 3121–3132.

Remus, D., Beuron, F., Tolun, G., Griffith, J.D., Morris, E.P., and Diffley, J.F. (2009). Concerted loading of Mcm2-7 double hexamers around DNA during DNA replication origin licensing. Cell *139*, 719–730.

Ruzankina, Y., Pinzon-Guzman, C., Asare, A., Ong, T., Pontano, L., Cotsarelis, G., Zediak, V.P., Velez, M., Bhandoola, A., and Brown, E.J. (2007). Deletion of the developmentally essential gene ATR in adult mice leads to age-related phenotypes and stem cell loss. Cell Stem Cell *1*, 113–126.

Shima, N., Alcaraz, A., Liachko, I., Buske, T.R., Andrews, C.A., Munroe, R.J., Hartford, S.A., Tye, B.K., and Schimenti, J.C. (2007). A viable allele of Mcm4 causes chromosome instability and mammary adenocarcinomas in mice. Nat. Genet. *39*, 93–98.

Sugimoto, N., Yugawa, T., Iizuka, M., Kiyono, T., and Fujita, M. (2011). Chromatin remodeler sucrose nonfermenting 2 homolog (SNF2H) is recruited onto DNA replication origins through interaction with Cdc10 protein-dependent transcript 1 (Cdt1) and promotes pre-replication complex formation. J. Biol. Chem. *286*, 39200–39210.

Swarnalatha, M., Singh, A.K., and Kumar, V. (2012). The epigenetic control of E-box and Myc-dependent chromatin modifications regulate the licensing of lamin B2 origin during cell cycle. Nucleic Acids Res. *40*, 9021–9035.

Wong, P.G., Glozak, M.A., Cao, T.V., Vaziri, C., Seto, E., and Alexandrow, M. (2010). Chromatin unfolding by Cdt1 regulates MCM loading via opposing functions of HBO1 and HDAC11-geminin. Cell Cycle *9*, 4351–4363.

Ying, Q.L., Stavridis, M., Griffiths, D., Li, M., and Smith, A. (2003). Conversion of embryonic stem cells into neuroectodermal precursors in adherent monoculture. Nat. Biotechnol. *21*, 183–186.

Stem Cell Reports

Supplemental Information

Embryonic Stem Cells License a High Level of Dormant Origins to Protect the Genome against Replication Stress

Xin Quan Ge, Jinah Han, Ee-Chun Cheng, Satoru Yamaguchi, Naoko Shima, Jean-Leon Thomas, and Haifan Lin

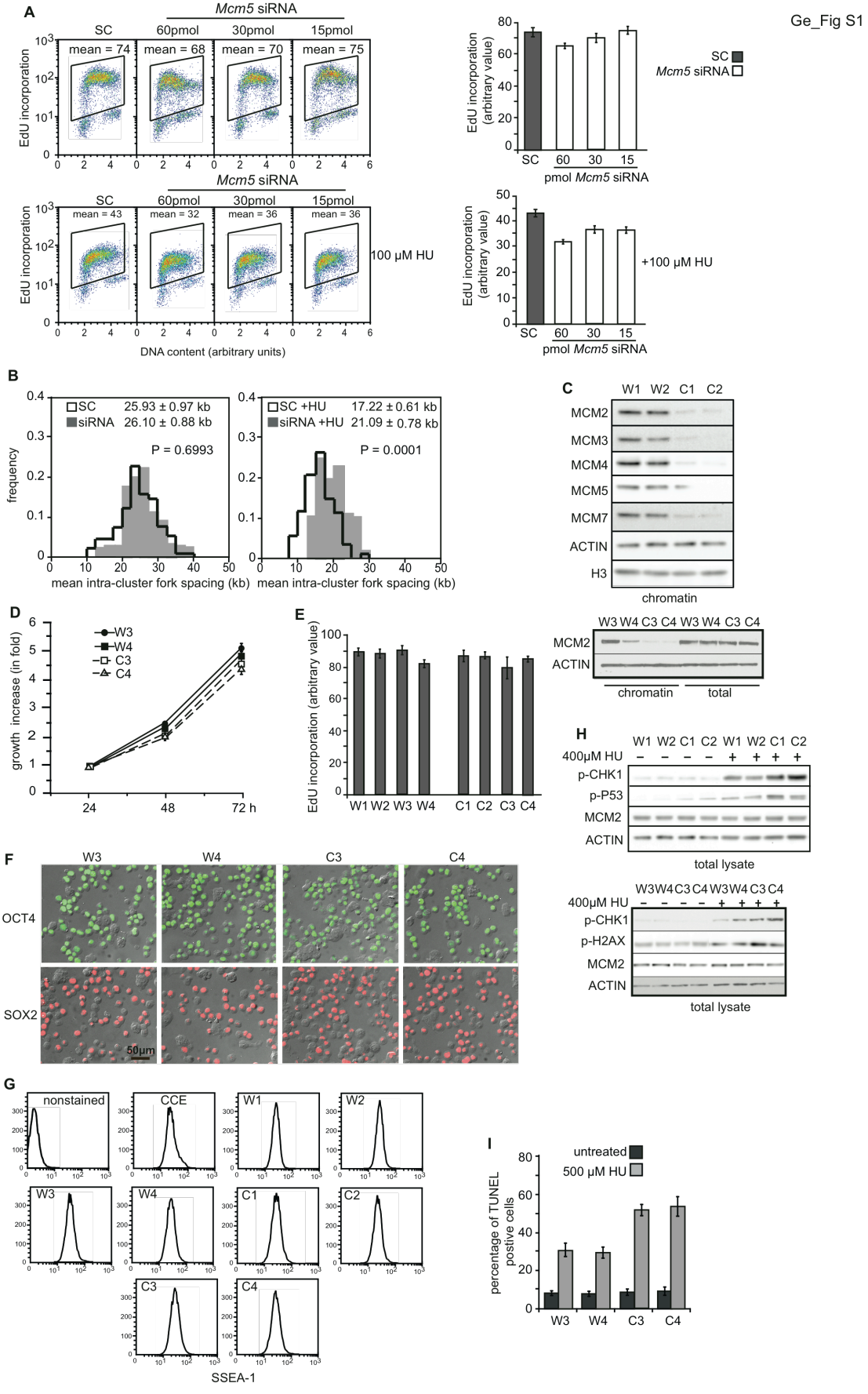
A
Mcm5 siRNA
SC
60pmol
30pmol
15pmol
mean = 74
mean = 68
mean = 70
mean = 75
EdU incorporation
mean = 43
mean = 32
mean = 36
mean = 36
100 μM HU
DNA content (arbitrary units)
EdU incorporation (arbitrary value)
SC
Mcm5 siRNA
pmol Mcm5 siRNA
+100 μM HU
B
SC 25.93 ± 0.97 kb
siRNA 26.10 ± 0.88 kb
P = 0.6993
SC +HU 17.22 ± 0.61 kb
siRNA +HU 21.09 ± 0.78 kb
P = 0.0001
frequency
mean intra-cluster fork spacing (kb)
C
W1 W2 C1 C2
MCM2
MCM3
MCM4
MCM5
MCM7
ACTIN
H3
chromatin
W3 W4 C3 C4 W3 W4 C3 C4
MCM2
ACTIN
chromatin
total
D
W3
W4
C3
C4
growth increase (in fold)
24
48
72 h
E
EdU incorporation (arbitrary value)
W1 W2 W3 W4 C1 C2 C3 C4
H
W1 W2 C1 C2 W1 W2 C1 C2
400μM HU
p-CHK1
p-P53
MCM2
ACTIN
total lysate
W3W4C3C4 W3W4C3C4
400μM HU
p-CHK1
p-H2AX
MCM2
ACTIN
total lysate
F
W3
W4
C3
C4
OCT4
SOX2
50μm
G
nonstained
CCE
W1
W2
W3
W4
C1
C2
C3
C4
SSEA-1
I
untreated
500 μM HU
percentage of TUNEL postive cells
W3
W4
C3
C4

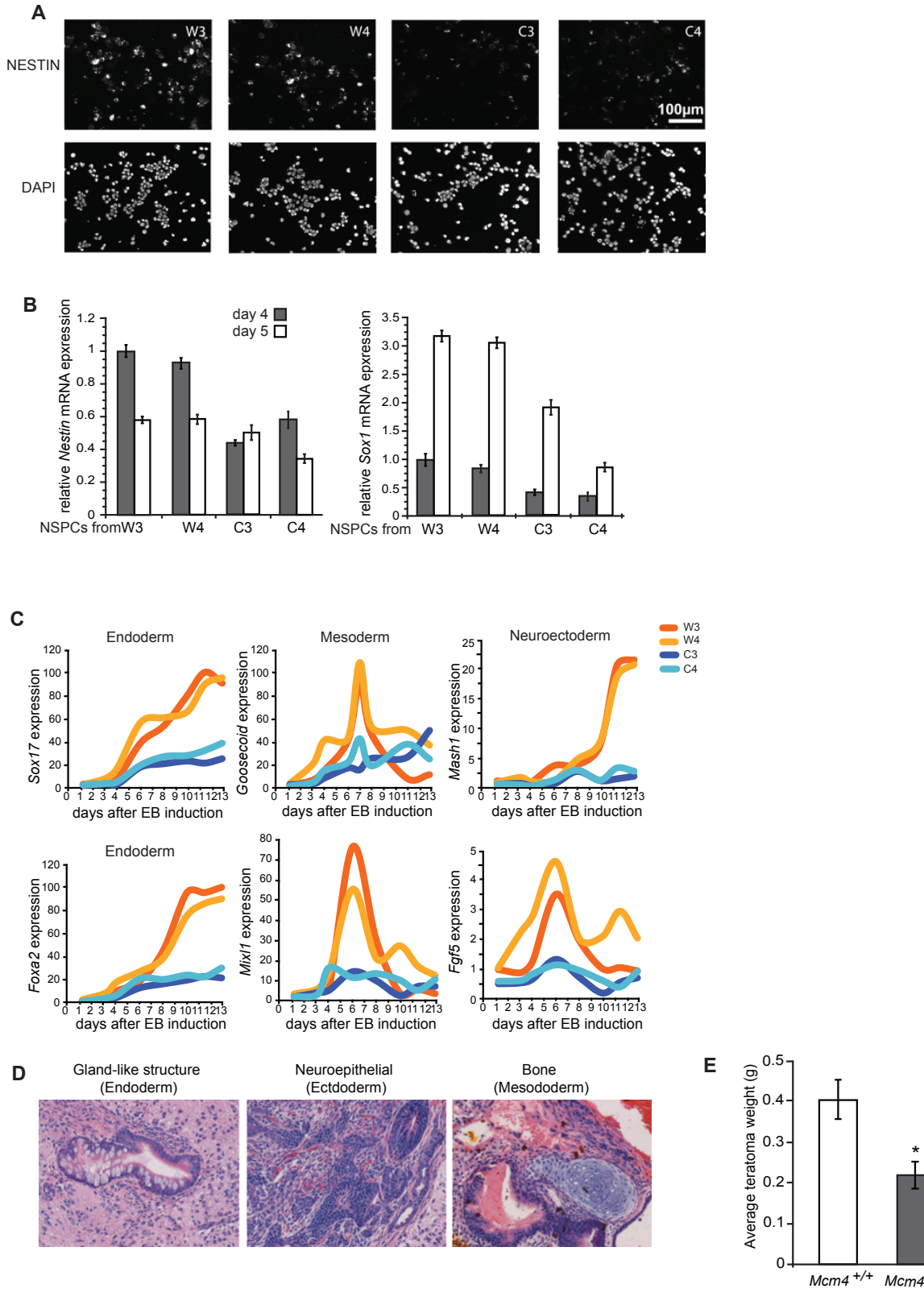
A
NESTIN
DAPI
W3
W4
C3
C4
100μm
B
day 4
day 5
relative Nestin mRNA epxression
NSPCs fromW3
W4
C3
C4
relative Sox1 mRNA epxression
NSPCs from W3
W4
C3
C4
C
Endoderm
Mesoderm
Neuroectoderm
Sox17 expression
Goosecoid expression
Mash1 expression
days after EB induction
W3
W4
C3
C4
Endoderm
Foxa2 expression
Mixl1 expression
Fgf5 expression
days after EB induction
D
Gland-like structure
(Endoderm)
Neuroepithelial
(Ectdoderm)
Bone
(Mesododerm)
E
Average teratoma weight (g)
Mcm4 +/+
Mcm4 C/C
*

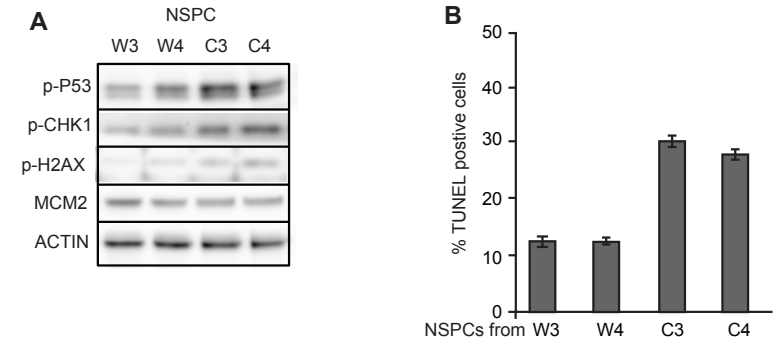
A
NSPC
W3 W4 C3 C4
p-P53
p-CHK1
p-H2AX
MCM2
ACTIN
B
% TUNEL postive cells
50
40
30
20
10
0
NSPCs from W3 W4 C3 C4

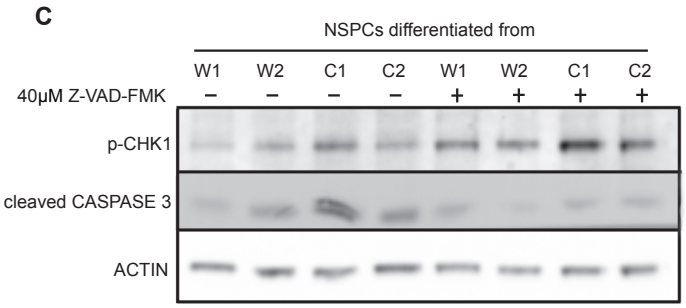
C
NSPCs differentiated from
W1 W2 C1 C2 W1 W2 C1 C2
40μM Z-VAD-FMK
− − − − + + + +
p-CHK1
cleaved CASPASE 3
ACTIN

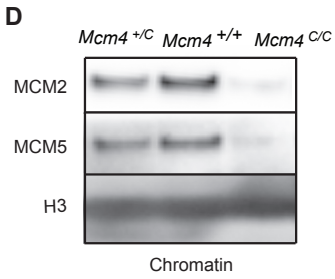
D
Mcm4 +/C
Mcm4 +/+
Mcm4 C/C
MCM2
MCM5
H3
Chromatin

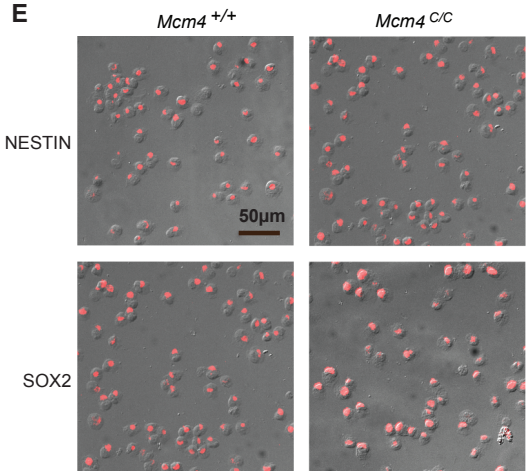
E
Mcm4 +/+
Mcm4 C/C
NESTIN
SOX2
50μm

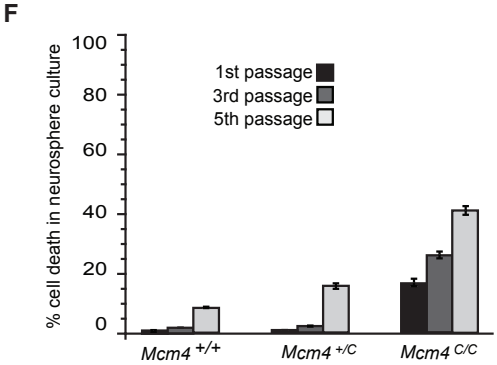
F
% cell death in neurosphere culture
100
80
60
40
20
0
1st passage
3rd passage
5th passage
Mcm4 +/+
Mcm4 +/C
Mcm4 C/C

A

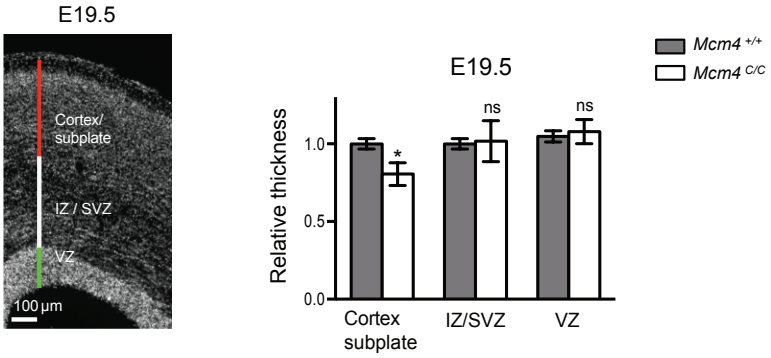

B

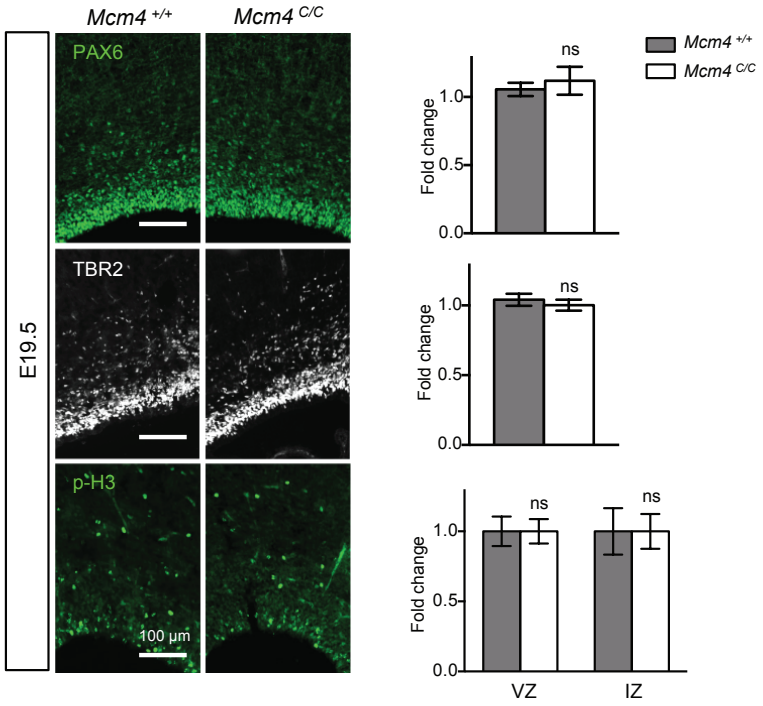

C

	Expected	Observed
Mcm4 $^{+/+}$	25%	40% (36/89)
Mcm4 $^{Chaos/+}$	50%	49% (44/89)
Mcm4 $^{Chaos/Chaos}$	25%	10% (9/89)

Supplemental Figure Legends

Figure S1. DO reduction does not affect ESC self-renewal, related to Figure 2.

(A) CCE ESCs were transfected with a serial dilution of the *Mcm5* or scrambled siRNA. Overall rate of DNA replication was assayed in cells after EdU pulse followed by FACS analysis. Cells were treated with HU for 4 hs before the analysis. Mean EdU incorporation is quantified and plotted. Note that 15pmol *Mcm5* siRNA does not change the rate of DNA replication, but make cells hypersensitive to HU. (**B**) Distribution of the mean intra-cluster fork spacing in CCE cells transfected with scrambled siRNA (SC) or 15pmol *Mcm5* siRNA analyzed by DNA fiber assay. Cells were treated with 100μM HU for 4 hs before the analysis. Overall average fork spacing ± standard error of the mean (SEM) is calculated. (**C-I**) Comparison between the $Mcm4^{+/+}$ (W1-W4) and $Mcm4^{C/C}$ (C1-C4) ESCs. (**C**) Immunoblot assaying chromatin-bound and total MCM protein level. (**D**) Cell proliferation rate analyzed over 72hs. (**E**) Overall rate of DNA replication assayed by EdU pulse and FACS analysis. (**F**) Immunofluorescence of OCT4 and SOX2 in ESCs. The fluorescent images are overlaid with the DIC images. (**G**) SSEA-1 expression assayed by FACS with CCE cells as a positive control. (**H**) Immunoblot analysis on the total lysate of cells after treatment with 400μM HU for 4 hs. (**I**) TUNEL assay of cells after treatment of HU for 48 hs. Error bars in Figure S1A, D, E and I indicate SEM from three independent experiments.

Figure S2. Dormant origin reduction impairs ESC differentiation, related to Figure 2.

(A) Immunofluorescence of NESTIN on day 4 after induced NSPC differentiation from the ESCs. (**B**) qRT-PCR of *Nestin* and *Sox1* expression during NSPC differentiation from ESCs (day 4 and day 5 post-induction). (**C**) qRT-PCR of the markers representing three germ

lineages during day 1 to day 13 of EB differentiation from the ESCs. (**D**) Representative images of endoderm, mesoderm and ectoderm tissues of teratomas generated from both the *Mcm4*$^{+/+}$ and *Mcm4*$^{C/C}$ ESCs. (**E**) The average weight of teratomas from four *Mcm4*$^{+/+}$ and four *Mcm4*$^{C/C}$ ESC lines. Two-tailed *t*-test: p = 0.0194. Error bars in Figure S2B and E indicate SEM from three independent experiments.

Figure S3. Dormant origin reduction impairs the differentiation of neural stem/progenitor cells (NSPCs), related to Figure 3.

(**A**) Immunoblot of NSPCs at 96 hs after induced differentiation from the *Mcm4*$^{+/+}$ (W3, W4) and *Mcm4*$^{C/C}$ ESCs (C3, C4). (**B**) TUNEL assay of NSPCs at 96 hs after induced differentiation from ESCs. Error bars represent SEM from three experiments. (**C**) Immunoblot showing the effect of CASPASE inhibitor Z-VAD-FMK on the levels of phospho-CHK1 and cleaved CASPASE 3 in NSPCs differentiated from the *Mcm4*$^{+/+}$ (W1, W2) and *Mcm4*$^{C/C}$ ESCs (C1, C2). 40μM Z-VAD-FMK was added at 48 hs after induced differentiation, and NSPCs were analysed at 96 hs. **(D**) Immunoblot of chromatin bound MCMs in the NSPCs from the embryo brains. (**E**) Immunofluorescence of NESTIN and SOX2 in the neurospheres generated from the NSPCs of embryo brains. The fluorescent images are overlaid with the DIC images. (**F**) Percentage of dead cells measured by trypan blue exclusion in the clonogenic neurosphere culture. Error bars in Figure S3B and F indicate SEM from three independent experiments.

Figure S4. The *Mcm4*$^{Chaos3/Chaos3}$ mutant displays thinner cortical layers, without neurogenesis alteration, at late embryonic stage E19.5, related to Figure 4.

(A) DAPI staining and measurement of the successive cortical zones. Note that outer layers (cortex and subplate) are thinner in the *Mcm4*$^{C/C}$ mutants, without alteration of the VZ and IZ/SVZ layers. **(B**) Immunolabeling of VZ/SVZ cells (PAX6^{+}), intermediate progenitor cells (TBR2^{+}) and dividing cells (p-H3^{+}) on coronal sections of the cortex. At late-stage neurogenesis, MCM4 partial loss-of-function does not affect the number of ventricular stem cells, intermediate progenitors and dividing cortical cells. lv: lateral ventricles. Error bars represent SEM of three independent experiments totaling 4 *Mcm4*$^{+/+}$ and 7 *Mcm4*$^{C/C}$ embryos. Two-tailed *t*-test: non-significant (ns), $p < 0.05$ (*). **(C)** Expected and observed frequencies of wild-type, heterozygote and homozygote embryos after self-crossing of the *Mcm4*$^{+/C}$ mice.

Supplemental Experimental Procedures

ES cell derivation and culture

Feeder-free CCE mouse ESCs were grown in standard ES cell culture medium consisting of high glucose DMEM supplemented with 15% ES cell-qualified fetal bovine serum, 2 mM L-Glutamine, 0.1 mM non-essential amino acids, 1 mM sodium pyruvate, 0.1 mM Monothioglycerol and 1000 U/ml LIF at 37°C, 5% CO_2. *Mcm4*$^{chaos3/chaos3}$ and wide-type mouse ESC lines were derived from the blastocysts generated by crossing *MCM4*$^{chaos3/+}$ heterozygous mice using previously described procedures (Bryja et al. 2006). They were maintained on mouse embryonic fibroblast (MEF) feeder layer in standard ES cell culture medium. Before experiments, feeders were removed and ES cells were grown on plates coated with 0.1% gelatin.

Mice

129/Sv mice were purchased from Taconic. *Mcm4*^{Chaos3} mice (C57BL/6J and C3HeB/FeJ mixed background) were maintained as heterozygotes. All experiments involving mice were approved by the Institutional Animal Care and Use Committee (IACUC).

Neural stem/progenitor cell culture

NSPCs were isolated and cultured as previously described (Saxe et al. 2007). Briefly, NSPCs were isolated from the forebrain of E13.5 mice. They were dissociated into single cells and cultured as neuropsheres by plating 50,000 cells/ml in DMEM/F12 media supplemented with B27, 1,000U/mL penicillin-streptomycin, 20ng/ml bFGF, 50ng/ml EGF and 2ug/ml heparin. For clonal neurosphere assays, dissociated single cells were re-plated at 1,000 cells/ml in 6 well plates in neurobasal medium with B27, 2mM L-glutamine, 1,000U/ml penicillin-streptomycin, 20ng/ml bFGF, 2ng/ml EGF, and 2ug/ml heparin. Neurosphere culture on day 6 was dissociated into single cells and plate at 1,000 cells/ml to initiate a new round of neurosphere growth.

Antibodies, chemicals and siRNA

Antibodies used were: phospho CHK1 ser345 (2341, Cell Signaling), phospho H2AX ser139 (2577, Cell Signaling), phospho P53 ser15 (9284, Cell Signaling), β-ACTIN (4967, Cell Signaling), H3 (4499, Cell Signaling), MCM2 (BM28, BD), MCM3 (4012, Cell signaling), MCM4 (ab4459, Abcam), MCM5 (ab75975, Abcam), MCM7 (ab2360, Abcam), SSEA-1 (560127, BD), cleaved CASPASE 3 (9661, Cell Signaling), NESTIN (clone 10C2, Millipore), OCT4 (C-10, Santa Cruz), SOX2 (560292, BD), PAX6 (Millipore (AB2237), Phospohistone

H3 (Millipore 06-570), TBR1 (Abcam ab31940), TBR2 (eBioscience 14-4875-82), Hydroxyurea (Sigma), Aphidicolin (Sigma), caffeine (Sigma) or Z-VAD-FMK (Sigma) were added to the medium, incubation time and concentrations of which were indicated in the results section. *Mcm5* siRNA (5'-CGAGCAUUCGGAUUCUGAATT-3') as well as scrambled siRNA (Dharmacon) were transfected into ES cells using a protocol adapted from siRNA transfection in human embryonic stem cells (Ma et al. 2010). Briefly, 60 pmol of siRNAs were mixed with 5 µl of Lipofectamine 2000 (Invitrogen) and then diluted in 100µl of OPTI-MEMI (Invitrogen). Cell pellet (1×10^6 cells) were then incubated in the resulting 100 µl of transfection solution for 15 min before seeded in standard growth medium. Cells were analyzed 72 hs after siRNA transfection.

DNA fiber analysis

DNA fiber analysis was carried out as previously described (Ge et al. 2007). Briefly, ES cells and neural stem/progenitor cells were pulsed with 50µM BrdU for 10min (without HU) or 20min (in presence of 100µM HU) in order to achieve examinable track length after spreading. Cells were then harvested and DNA fiber spread was prepared. For immunodetection of BrdU labeled tracks, acid treated fiber spreads were incubated with mouse anti-BrdU (BD) and Alexa Fluor 555-conjugated rabbit anti-mouse IgG. DNA fibers were examined using Zeiss microscope using 65x lens. Fibers containing at least four consecutive tracks within the range of expected length were selected for analysis, and average track spacing was determined. For each sample, at least 50 measurements were performed giving rise to overall fork spacing ± standard error of the mean (SEM).

Examination of chromatin-bound MCM2-7 complexes

To assay chromatin-bound MCMs by immunoblot, experiments were performed as previously described (Ge et al. 2007). Briefly, cells were incubated with cytoskeleton (CSK) buffer supplemented with 0.2% triton for 10 min on ice. Cells were then centrifuged at 5000g for 5min to obtained pellet containing chromatin-bound proteins. The pellets were suspended in Nupage LDS sample buffer (Invitrogen, supplemented with 5% 2-mercaptoethal) and subject to immunoblot. To assay chromatin bound MCM2 by FACS, cells were incubated with CSK buffer supplemented with 0.2% triton for 10min on ice, centrifuged at 400g for 5min and fixed with 2% paraformaldehyde at 37 ^{o}C for 10min. MCM2 was labeled with primary mouse antibody (347580, BD) and Alexa Fluor 488-conjugated rabbit anti-mouse IgG. DNA was labeled with 20μg/ml 7AAD, and all samples were analysed using a FACSCalibur flow cytometer (BD) and Flowjo software. To quantify chromatin bound MCM2 in G1 phase, the geographical mean of immunolabeled MCM2 was calculated (since the data is collected on a logarithmic scale).

Immunofluoresence

ESCs and neural stem cells were harvested and trypsinized into single cells before the experiments. Cells were than fixed with 2% paraformaldehyde for 10 minutes at room temperature and cytospined onto microscope slides. After permeabilization with 0.2% triton for 10min, cells were stained with primary and secondary antibody as described in the above section.

Tissue collection, immunohistochemistry and data analysis

Pregnant mice (stage of pregnacy E13.5, 15.5 and 19.5) were anaesthetized with

isoflurane inhalation and embryos were removed from the uterus. Embryonic heads (E13.5) and brains (E15.5 and 19.5) were fixed by immersion in 4% paraformaldehyde in PBS, pH7.4 overnight at 4°C. After washing in PBS, samples were soaked overnight at 4°C in 20% sucrose in PBS to cryoprotect the tissues. Brain coronal cryosections (20 μm thick) were sequentially incubated with blocking solution (Dako X0909) for 1 hr at room temperature, primary antibodies diluted in PBS containing 0.1~1% Triton X-100 for overnight at 4°C, and secondary antibodies for 3 hrs at 4°C. Cell nuclei were co-stained by DAPI and slides were mounted with Fluoromount (Southern Biotechnologies Associates). Images were acquired on a Nikon ECLIPSE 80i microscope and ImageJ was used for quantification. For quantification of the cortical and ventral forebrain size, coronal sections were selected at the same anterior-posterior level of the forebrain, just rostral to the anterior emergence of the corpus callosum. In each embryo, three measurements were performed on 4x images, on both the left and the right hemisphere. For quantification of cell number, 10x images were taken. TBR2, p-H3 and cleaved-CASPASE 3 positive cells were counted, and the thickness of PAX6 and TBR1 cell layer was measured.

Super-resolution 3D structured illumination microscopy

Cells were synchronized by incubation in 2.5 mM thymidine for 12 hs followed by 50ng/ml of nocodazole for 7 hs. Cells were then released for 2 hs into G1 phase and chromatin-bound MCMs were extract using methods described in this paper. MCM proteins were labeled with primary antibodies and Alexa Fluor 568-conjugated rabbit anti-mouse or rabbit IgG. To image MCM foci in cells, Delta Vision OMX imaging system (Applied Precision) was used to collect 125nm serial Z sections using a 63× NA 1.4 lense. SoftWorx was used to process raw images for reconstruction to reveal structures in three dimensions.

3D image stacks were then analyzed with Volocity (PerkinElmer) where a threshold-based segmentation was applied to define MCM foci. The same degree of threshold was used across different samples to cover 90% of all visually defined foci in each cell. To calculate cellular foci number, >100 cells pooled from three sets of experiments were used to generate mean foci number and SEM.

DNA synthesis, cell growth and TUNEL assay

To assay the rate of DNA synthesis, cells were labeled with 10 μM EdU for 30 min and stained according to manufacturer's instruction (Click-iT^{TM} EdU Alexa Fluor 647 Flow Cytometry, Invitrogen). DNA was stained with 20 μg/ml 7AAD. All samples were analyzed using a FACSCalibur flow cytometer (BD) and Flowjo software. To quantify EdU incorporation, the geographical mean of incorporated EdU was then calculated (since the data is collected on a logarithmic scale), from which the overall rate of DNA synthesis was derived. Cell growth rate was assayed with the alamarBlue CellViability Reagent (Invitrogen). Absorbance was measured at 570 and 600 nm. Apoptosis of the samples was assayed by ApopTag Fluorescein *in situ* Apoptosis Detection Kit according to the manufacturer's instruction (Millipore).

ESC differentiation and quantitative RT-PCR

Neural stem/progenitor cell (NSPC) differentiation was performed as previously described using N2B27 medium (Ying et al. 2003). NSPCs were harvested on day 4 to day 6 after induction of differentiation depending on different experiments. Embryoid body differentiation was achieved by hanging drop method as described previously (Jackson et al. 2010). Teratoma assay was performed by injecting one million ES cells subcutaneously into

six to eight-week-old SCID-beige mice as previously described (Wesselschmidt 2011). Three weeks post-injection, teratomas were harvested, fixed and stained with hematoxylin and eosin for histological analysis. For quantitative RT-PCR analysis of gene expression, total RNA was extracted using RNeasy Plus Kit (Qiagen), reverse transcribed and amplified by lineage specific primers (*Nestin, Sox1, Sox17, Goosecoid, Mash1, Fgf5, Mixl1, Foxa2*) as previously described (Ivanova et al. 2006; Kwon et al. 2014). *Gapdh* was used as internal control for qRT-PCR, and signals in each sample was normalized against it. Primer sequences:

Nestin – For; 5′-CCAGAGCTGGACTGGAACTC-3’, Rev; 5′-ACCTGCCTCTTTTGGTTCCT-3’

*Sox1 – For; 5’-*ATGCACCGCTACGACATGGG-3’, Rev; 5’-GCTCCGACTTGACCAGAGATCC-3’

*Sox17 – For; 5’-*AAGAAACCCTAAACACAAACAGCG-3’,

Rev; 5’TTTGTGGGAAGTGGGATCAAGAC-3’

Goosecoid – For; 5′- AAACGCCGAGAAGTGGAACAAG-3’,

Rev; 5′- AAGGCAGGGTGTGTGCAAGTAG-3’

Mash1 – For; 5′-TAACTCCAAACCACTAACAGGC -3’, Rev; 5′-TGAGGAAAGACATCAACGCAGT-3’

Fgf5 – For; 5′-CTGTATGGACCCACAGGGAGTAAC -3’, Rev; 5′- ATTAAGCTCCTGGGTCGCAAG-3’

Mixl1 – For; 5′-TTGAATTGAACCCTGTTGTCCC-3’, Rev; 5′- GAAACCCGTTCTCCCATCCACC-3’

Foxa2 – For; 5′-GGCACCTTGAGAAAGCAGTC-3’, Rev; 5′-GACATACCGACGCAGCTACA-3’

Gapdh – For; 5′-TCCCACTCTTCCACCTTCGATGC-3’,

Rev; 5′- GGGTCTGGGATGGAAATTGTGAGG-3’

Supplemental References

Bryja, V., S. Bonilla, and E. Arenas. 2006. Derivation of mouse embryonic stem cells. *Nature protocols*. 1:2082-2087.

Ivanova, N., R. Dobrin, R. Lu, I. Kotenko, J. Levorse, C. DeCoste, X. Schafer, Y. Lun, and I.R. Lemischka. 2006. Dissecting self-renewal in stem cells with RNA interference. *Nature*. 442:533-538.

Jackson, M., A.H. Taylor, E.A. Jones, and L.M. Forrester. 2010. The culture of mouse embryonic stem cells and formation of embryoid bodies. *Methods Mol Biol*. 633:1-18.

Kwon YR, Jeong MH, Leem YE, Lee SJ, Kim HJ, Bae GU, Kang JS. 2014. The Shh coreceptor Cdo is required for differentiation of midbrain dopaminergic neurons. *Stem cell research* **13**: 262-274.

Ma, Y., J. Jin, C. Dong, E.C. Cheng, H. Lin, Y. Huang, and C. Qiu. 2010. High-efficiency siRNA-based gene knockdown in human embryonic stem cells. *Rna*. 16:2564-2569.

Saxe, J.P., H. Wu, T.K. Kelly, M.E. Phelps, Y.E. Sun, H.I. Kornblum, and J. Huang. 2007. A phenotypic small-molecule screen identifies an orphan ligand-receptor pair that regulates neural stem cell differentiation. *Chemistry & biology*. 14:1019-1030.

Wesselschmidt, R.L. 2011. The teratoma assay: an in vivo assessment of pluripotency. *Methods Mol Biol*. 767:231-241.

Ying, Q.L., M. Stavridis, D. Griffiths, M. Li, and A. Smith. 2003. Conversion of embryonic stem cells into neuroectodermal precursors in adherent monoculture. *Nature biotechnology*. 21:183-186.